Research Article

Voltage and Frequency Control in a Microgrid

Obaid Siddiqui[1], Ward Ul Hijaz Paul[1,*], Sheeraz Kirmani[2], Mubassir Ahmad[1], Danish Ali[1] and Md Safdar Ali[1]

[1]*Jamia Millia Islamia, New Delhi, India*
[2]*Aligrah Muslim University, Aligrah, UP, India*

_____

Abstract

Microgrid provides a replacement of combining renewable energy resources and distributed generation units into power systems in an efficient manner. For the deployment of a microgrid, its stability and control issues are to be taken care of. Various efforts are being made to design more efficient control methods in different types of control types and different types of protection programme to make a reliable, safe, and economical operations of microgrid which is operated in either grid-connected mode or islanded operation mode. In the first stage of implementation, inner current control loop is designed along with phased locked loop and its effect is studied using a Simulink model in Matlab. In the second stage of implementation, outer control loop is designed, and its simulation is obtained along with PQ block. At the latter stage a VSC model is implemented serving with VF control using Matlab and its response is taken. In the final stage of implementation, power sharing methods V-F and Q-E are discussed. Two VSCs serving a load using the droop control is studied and Simulink model is made and implemented.

Keywords: Microcrid, Control, RES, VSC

_____

1. Introduction

Microgrid (MG) provides an alternative that the renewable energy sources (RESs) and distributed generations (DGs) are facing in integrating into the power systems. The stability and the implementation of a control system must be taken care of in order to deploy an MG. Research is being carried out on the construction of more effective control topologies in various control layers and protection techniques to ensure that MG operations in grid linked or shielded operating mode are powerful, secure and economical.

The most relevant challenges in MG are its uncertainties, low inertia, dynamic modelling and its stability, bidirectional power flow etc. In grid-connected mode of operation how the interaction of MG with the main grid are being considered while reliability and control issues are taken into account in islanded mode of operation [1].

Various control loop methods are being used to improve MG's stability and performance. The feedback variables that are used in MG loops for both grid connected, and islanded operations are mainly current, voltage/amplitude, frequency/angle, active and reactive powers. The hierarchical management system for MG guarantees the correct load sharing, voltage / frequency regulation, and power transfer between MG and the main grid and the surrounding grids in all operating modes.

Hierarchical control programme contains 4 levels of operations, namely local, secondary, global controls and emergency, as shown in Fig 1. The local programme contains basic control structure in which voltage and current control loops of DGs are present which measures the local signals and helps in maintaining the MG stability.

The secondary control provides power sharing for parallel layout of DGs and makeup for the frequency and voltage variation which occurs when the load changes [2]. The emergency level of operations smoothens the MG supervision role. This control scheme is important in islanding operations. It is responsible for connection/disconnection to/from the main grid and is also used in microgrid energy management system (EMS)..The final control is the global control which regulates the flow of power between the MG, interconnecting MG and the main grid. This type of control scheme mainly used in distribution area, outside the MG. The MG also participates in the regulation of the distribution network by regulating the active and reactive powers by taking different control loop algorithms.

One of the schemes is controlling the voltage and frequency of a microgrid through a voltage source converter (VSC). VSC is used as an interface between the distributed energy networks and the MG.
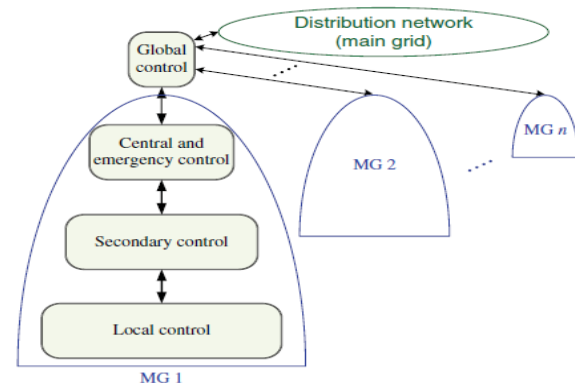

Fig. 1. Different control levels in microgrid.

_____

1.1. Microgrid and its structure

The microgrid structure includes various types of distributed energy resources, like PV panel, fuel cells, wind turbines, storage units such as flywheels, super-capacitors, batteries etc. These types of systems are mainly operated in LV distribution region and can also operate in islanded mode in case of fault in the main network [3]. MGs are very economical in customer's point of view as it produces both thermal and electrical supplies and also improves the quality of power by reducing the voltage fluctuations thereby reducing the cost of electricity [4].

As the energy supplied by the DESs keeps on fluctuating, backup power supplies are required to have a good level of energy reliability. Taking an example, diesel generators are used along with wind turbine and fuel cells for seamless power supply. In some areas, PV-Wind structure is used as we know PV panel will produce more power during daytime and wind turbines produces more generation with powerful winds during nighttime [5]. With the introduction of energy storage devices along with the DERs it ensures reliable and efficient power supply.

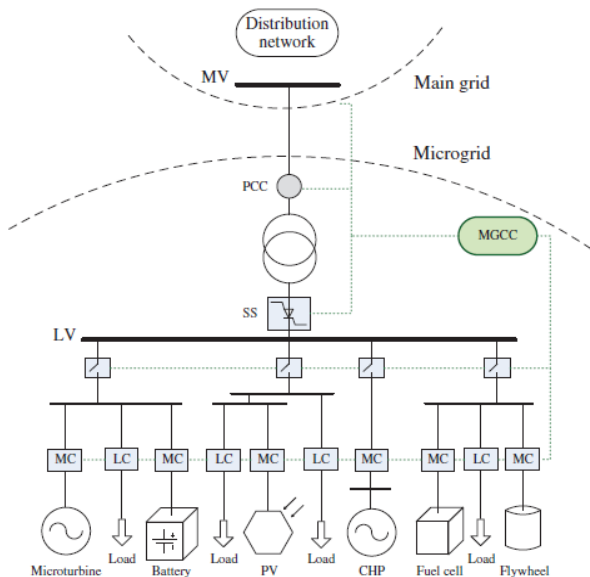A general model of MG can operate in both grid connected and islanded mode as shown in figure 2.

Fig. 2. A basic SLD of microgrid.

In grid connected mode, since it is used to supply local loads inside the MG and there is a flow of power from microgrid to main grid which made it a bit complex operation. A microgrid network is radial in nature with many feeders connected to it as shown in figure 3. In a radial network, each feeder consists of circuit breaker and power flow controller. The function of CB is used to isolate the feeder from the microgrid in case of disturbances occurring through it. Generally, microgrid is connected to the distribution network at the PCC through Secondary Switch (SS). The SS is used to isolate the microgrid for maintenance objectives or when fault take place.

The microgrid network consists of LV systems, loads, handleable and un-handleable power supplies and energy storage units. The control structure is based upon of communication system which is used to monitor the power generated by generators and power consumed by the load.

The balance between the demand and generation is the main important thing for the microgrid management both in grid connected mode and the islanded mode.
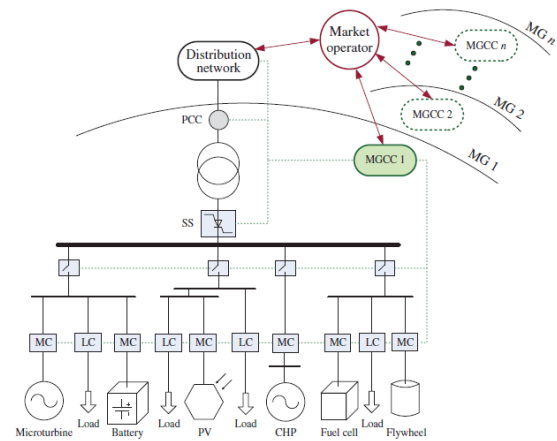

Fig. 3. A general version of microgrid controls.

1.2. Microgrid infrastructure

1.2.1. AC microgrid infrastructure

Exiting grid systems and loads are AC in nature and AC can easily be step up or step down using step up/down transformer.

As microgrids are preferably placed in the distribution systems it is interface with the grid through point of common coupling (PCC) through which two type of mode can be implemented i.e., grid connected mode and islanded mode. Distributed Energy Resources (DER) like photovoltaic (PV) produces DC power which is fed to the DC-AC converter and is connected to AC bus [6]. Energy storage is very important in microgrid architecture as the power produces by the DGs are intermittent. Its major role is to absorb surplus power and can supply to the load when the power produced by the DGs are insufficient, therefore it requires a bidirectional converter for charging or discharging. There are mainly two types of load connected for domestic purposes: AC load and DC load. AC load like induction motors is directly connected to the AC bus but the DC loads require a rectifier before it. Other type of DGs like wind turbine is directly connected to the AC bus through an AC-AC converter [7].

These type of microgrid are widely used as it is very convenient to integrate with the present grid systems and the load supply. The major disadvantage of AC microgrid is the synchronization with the main grid as frequency, phase angle, voltage needs to get matched with the main grid. Thus, power quality demand is more in AC microgrid than DC microgrid as only voltage in DC bus needs to be controlled. In DC microgrid synchronization is much easier [8]. Thus, the layout of AC microgrid is much more complicated than DC microgrid as number of transformations required is more which therefore reduces the system reliability.

1.2.2. DC microgrid infrastructure

DC microgrid is becoming a new vision of technology due to increase in the consumption of DC load like laptops, mobile phones and various electronic devices. On a similar note, to AC microgrid it is connected to the main grid through point of common coupling which enables connection and disconnection [9]. DC distributed generators like photovoltaic, energy storage devices and DC loads are directly connected to the DC bus through a DC-DC converter. AC loads like motors, generators require a rectifier to integrate with the DC bus [10], [11]. DC

microgrid is much more efficient than AC as the power conversion losses is very less. As there are very less conversion blocks DC microgrid is more reliable and has a simple architecture.

The main drawback of DC microgrid is that the existing AC network is very hard to re-use as a DC network. Thus, it is requiring reconstruction of the network which requires a high amount of investment. Protection is also highly complicated as AC network. It is also very difficult to step up and step down the voltages in the microgrid [12]. These type of networks are mainly used in telecommunications, spacecraft, data centre, etc.

1.2.3. Hybrid microgrid infrastructure

Hybrid microgrid comprises a pair of AC and DC microgrid connection. In these type of grids AC microgrid is directly connected to the PCC and the DC microgrid is connected to the AC bus via bidirectional AC/DC converter. A hybrid microgrid can also be called as an AC microgrid connected with a sub- DC microgrid. AC/DC converter is considered a main component between an AC microgrid and sub- DC microgrid [13]. Its main function is to manages the power flow between the two systems and also to maintain the DC bus voltage. Coordination control among the converters is the important factor to achieve efficiency and stability of the microgrid.

1.3. Control methods of microgrid

Microgrid contains different types of renewable types of sources like PV array, wind turbines. The energy from these types of sources is intermittent in nature. There should be an easy passage of power flow between the micro grid and the main grid, and the grid should also operate when disconnected from the main grid. As there are different type of renewable resources which is variable in nature therefore correct control methods are required to achieve the purpose. The scheme for microgrid control is as follows:

1. Easily integration of new distributed generators (DGs) with the existing microgrid.
2. Control of DG power and flow of the reactive power to the main grid when it is operating in grid connected mode.
3. There should be dynamic load sharing when the load switches in or out during islanded mode [14].
4. Maintaining power quality and keeping the voltage and frequency in the desirable limit.
5. To ensure stability o the system when fault or disturbances occur.
6. The transition to the islanded mode from the grid mode should be smooth occurring intentionally or unintentionally.

2. Control of Voltage Source Converter (Vsc)

For VSC control, cascaded control structure is being used. The inner loop is a current control loop, and the outer is power or voltage/frequency loop. The reason to have inner control as a current control because VSC is sensitive to large currents. The VSC can now be protected against over-current with the current loop. The inner loop control and the outer loop are designed separately as their bandwidth requirements are different. The inner loop requires a faster response and a higher bandwidth whereas, the outer loop requires a slower response and a much lower bandwidth

[15].

Design of inner current controller

The inner control loop is to design to have a much faster response than the outer loop. RL circuit is taken between the converter and the PCC as shown in figure 4. The equation is as follows:

$$L\frac{d\vec{i}}{dt} + R\vec{i} = \vec{v} - \vec{v_1} \tag{1}$$

Where $\rightarrow$ is the space vector.

$$L\frac{d(i_d + ji_q)}{dt} + jwl(i_d + ji_q) + R(i_d + ji_q) = v_d + jv_q - (v_{1d} - jv_{1q}) \tag{2}$$

Where w is the grid frequency, $v1_q = 0$ since PCC is aligned with the d-axis

Separating equation (2) into dq-axes, we get the following plant model:

$$L\frac{di_d}{dt} + Ri_d = v_d - v_{1d} + wLi_q \tag{3}$$

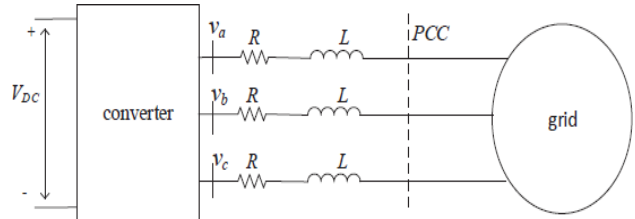$$L\frac{di_q}{dt} + Ri_q = v_q - v_{1q} - wLi_q \tag{4}$$

Fig. 4. A basic converter connected to a grid.

The plant model for the current controller from the above equation is calculated as $\frac{1}{R+sL}$ as for both d and q axes [16]. The inputs are i_d and i_q. The feedback control is designed to track the reference signals. The dq components of the converter voltage, cross coupling terms should be added after are obtained from the controllers.
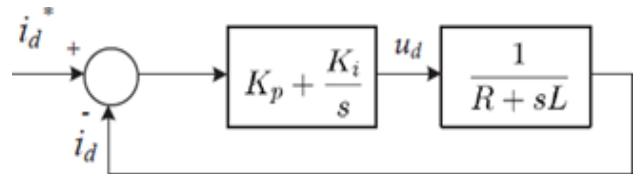Figure 5. shows the simple current control block.

Fig. 5. Simple block diagram for inner loop control.

The loop gain of the system is given by:

$$l(s) = \frac{k_p}{sL}\left(\frac{s + \frac{k_i}{k_p}}{s + \frac{R}{L}}\right) \tag{5}$$

An approximation is taken that plant pole is much closer to the origin. Thus, the plant pole is cancelled by the compensator's zero $\left(\frac{K_i}{K_p} = \frac{R}{L}\right)$. Thus, the loop gain becomes:

$$l(s) = \frac{k_p}{sL} \tag{6}$$

The closed loop transfer function is given by:

$$G_{Inner}(s) = \frac{l(s)}{1+l(s)} = \frac{1}{1+\tau s} \qquad (7)$$

Taking, R=.02Ω and L=0.04H and are calculated to be 50 and 100 respectively and the bandwidth comes around to be 2500 rad/s (τ=0.4ms).

2.1. Phased Locked Loop (PLL)

With the inner current loop, u_d and u_q will get produced. The converter dq-axis reference voltage is computed as follows:

$$v_d *= u_d + v_{1d} - wLi_q \qquad (8)$$

$$v_q *= u_q + v_{1q} + wLi_q \qquad (9)$$

For the generation of , $v_d *$ and $v_q *$ it requires the feed forward variable (v_d and v_q) along with the cross coupling terms ($-\omega L i_q$ in the $d-axis$ and $\omega L i_d$ in the $q-axis$). The space vector of the converter voltage is given as:

$$\vec{v} = (v_d + jv_q)e^{j\theta} \qquad (10)$$

Where θ is the PCC space vector's angle measured along the static reference frame. v_a, v_a, v_c be found from the space vector.

$$\begin{cases} v_d = \Re(\vec{v}) = v_d \cos\theta - v_q \sin\theta \\ v_d = \Re\left(\vec{v}e^{\frac{-j2\pi}{3}}\right) = v_d \cos\left(\theta - \frac{2\pi}{3}\right) - v_q \sin\left(\theta - \frac{2\pi}{3}\right) \\ v_c = \Re\left(\vec{v}e^{\frac{-j2\pi}{3}}\right) = v_d \cos\left(\theta + \frac{2\pi}{3}\right) - v_q \sin\left(\theta + \frac{2\pi}{3}\right) \end{cases} \qquad (11)$$
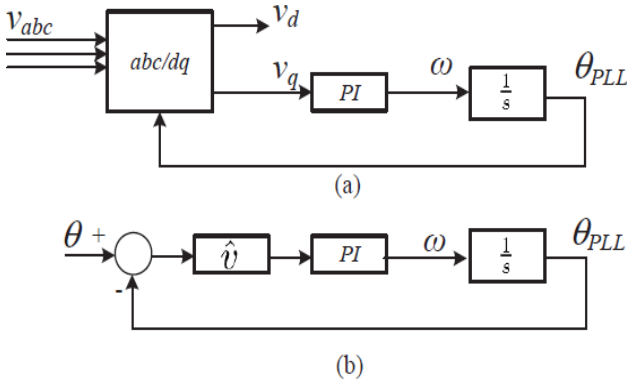

(a)

(b)

Fig. 6. (a). A simple block diagram of PLL. (b) Linearized block diagram of PLL.

We have designed PLL to have a bandwidth of 100 Hz. To test the design, linearized control blocks are used. Using the space vector technique, the input- output relationship is given as:

$$\begin{cases} v_d = (\hat{v}\cos(\theta - \theta_{PLL}) \\ v_q = (\hat{v}\sin(\theta - \theta_{PLL}) \end{cases} \qquad (12)$$

Assuming $\theta - \theta_{PLL} \approx 0$ the linearized model for v_q can now be expressed as:

$$v_q = -\hat{v}(\theta - \theta_{PLL}) \qquad (13)$$

Assuming the closed system is represented as in Figure 6(b),

$$\frac{\theta_{PLL}}{\theta} = \frac{K_P s + K_i}{s^2 + K_P s + K_i} \qquad (14)$$

Figure 7. show the closed system's bode plot. From the bode plot it is confirmed that peak value occurs at 100Hz. The bandwidth from the figure is approximately 100Hz.

A Simulink model is also built in figure 8. The Simulation results are shown in figure 9. The abc/dq block is build. v_d and v_q are from v_{abc} . The space vector is expressed in the terms of $v_{abc.}$
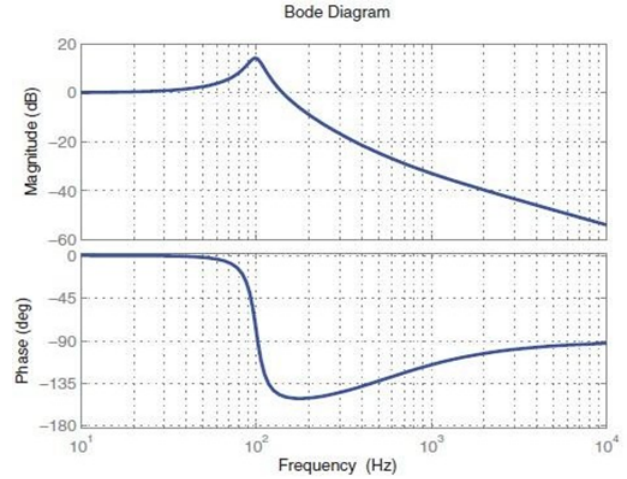

Fig.7. Bode plot for the system 2.14.
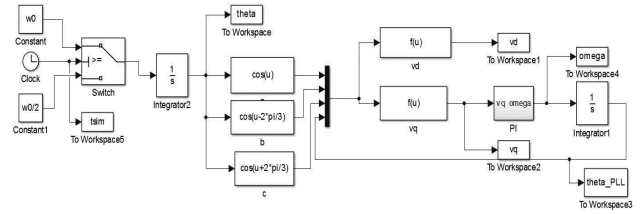

Fig. 8. A Simulink model for a PLL system.

Therefore,

$$\begin{cases} v_d = \frac{2}{3}\left(v_a \cos\theta_{PLL} + v_b \cos\left(\theta_{PLL} - \frac{2\pi}{3}\right) + v_c \cos\left(\theta_{PLL} + \frac{2\pi}{3}\right)\right) \\ v_q = \frac{2}{3}\left(v_a \sin\theta_{PLL} + v_b \sin\left(\theta_{PLL} - \frac{2\pi}{3}\right) + v_c \sin\left(\theta_{PLL} + \frac{2\pi}{3}\right)\right) \end{cases} \qquad (15)$$

The simulation results shows when there is a change of frequency in the input signal, the PLL is able to identify it and correct in within 0.05 seconds. The output angle of the PLL is able to track the given input angle [17]. The overall current control with the PLL is shown in figure 10, which consists of inner current control, PLL and outer PQ control. This type of control is recommended for grid integration.
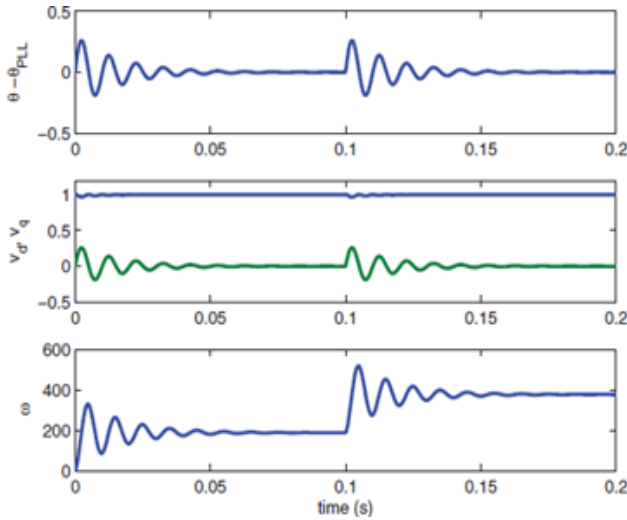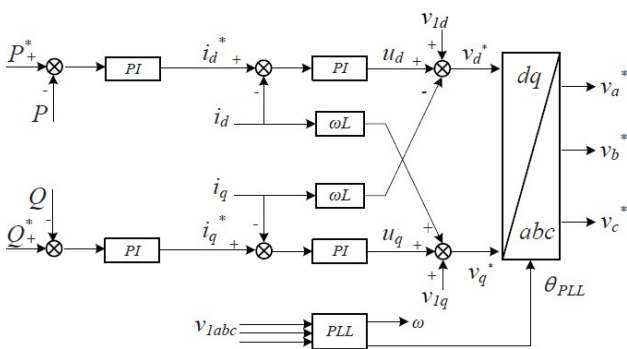
Fig. 9. Simulation results for figure 8.

Fig. 10. A VSC control structure.

2.2. Testing of current control and PLL

A MATLAB/SIMULINK is built to check the performance after designing the current control and PLL. The test model consists of the plant model (RL circuit), PLL, and the current controllers. The test bed is shown in figure 11. Three embedded MATLAB functions are used to convert from the given converter voltage, and the grid voltage, and the converter. The PCC voltage angle has been used as the input for the abc/dq or dq/abc conversion. PLL block is used to measure the angle of the PCC voltage. The inputs to the PLL are the voltage of the grid [18].
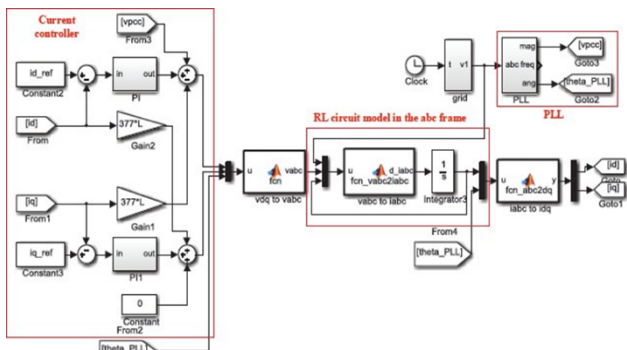

Fig. 11. Simulation diagram to validate the system with current controllers and PLL.

Reference dq currents are taken as constants. Initial value of the integrator is taken as zero. The simulation is given in figure in 12.
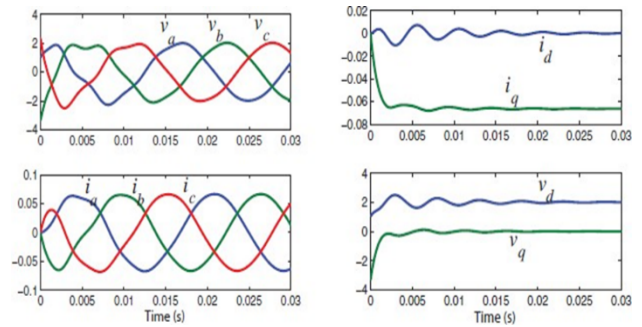

Fig. 12. Simulation result for current controller block and PLL.

From the above figure it is seen that within 0.03 seconds, the dq currents reach the steady state values.

3. Pv And Pq Control

3.1. Design of PV or PQ outer control
The outer loop is made to have a slow response compared to the inner current control loop. The simple schematic of the outer control loop is shown in figure 13.
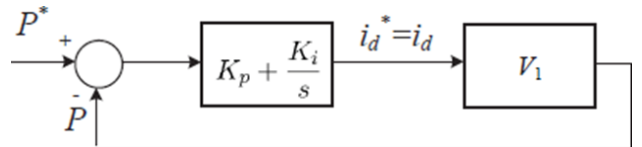

Fig. 13. Simple block diagram of outer loop control.

A closed transfer function is given as:

$$G_{outer}(S) = \frac{\left(k_p + \frac{k_i}{s}\right)v_1}{1 + \left(k_p + \frac{k_i}{s}\right)v_1} = \frac{\frac{k_p}{k_i}s + 1}{\left(\frac{1}{v_1 k_i} + \frac{k_p}{k_i}\right)s + 1} \qquad (16)$$

It is the first order transfer function in the form of $\frac{as+1}{\tau s+1}$ where τ is the time constant and the bandwidth is calculated as $1/\tau$ We are designing the outer loop with the value of $k_P = 0.1$ and $k_i = 5$, therefore the bandwidth comes out to be 4.5 rad/s. From this it can be seen that the bandwidth is 300 times slower than the inner current control loop.

3.2. AC voltage control
Ac voltage control is often used as a replacement to the Q-control. The main objective of the ac voltage control is to maintain the PCC voltage to a reference value. For this design, PCC and the grid should be connected to the line. If PCC voltage is the grid voltage, then there is no need to design [19]. The plant model can be formed as:

$$\Delta v_1 \approx \frac{\Delta Q}{S_{sc}} = \frac{v_1}{S_{sc}} \Delta i_q \qquad (17)$$

Where S_{sc} denotes the short circuit capacity.
The variation of voltage and the injection of the reactive power relationship is shown in figure 14.
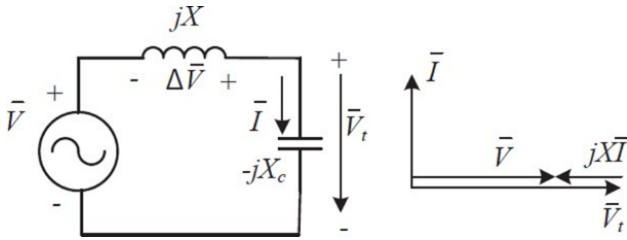
Fig. 14. Effect of Shunt reactance compensation.

Taking the compensator as a shunt capacitor with reactance is connected to the terminals. Therefore, the voltage gets increased by:

$$\Delta \vec{V} = \vec{V_t} - \vec{V} = -jX\vec{I} = -jX\frac{\vec{V_t}}{-jX_c}$$

$$\approx X\frac{\vec{V}}{X_c}, assuming \ change \ in \ voltage \ to \ be \ small$$

$$= \frac{Q}{S_{SC}} \tag{18}$$

The transfer function for the closed loop system is given as:

$$\frac{\Delta V_1}{\Delta V_1^{ref}} = \frac{k_p + \frac{k_i}{s}}{1 + \left(k_p + \frac{k_i}{s}\right)\frac{1}{S_{SC}}} = \frac{\frac{k_p}{k_i}s + 1}{\frac{k_p + S_{SC}}{k_i}s + 1}S_{SC} \tag{19}$$

Assuming is approximately equal to 1 pu. Thus, from the transfer function the bandwidth and time constant are calculated which is found to be:

$$\tau = \frac{k_p + S_{SC}}{k_i} \tag{20}$$

$$\omega_{bw} = \frac{1}{\tau} \tag{21}$$

Taking the bandwidth is 100 rad/s.

The Simulation diagram shown in figure 11 is modified to include a PQ controller. Figure 15 denotes the simulation outcomes at t=0.25s, the reference real power P* changes from 0 to 0.1 pu. At t=1s, reference reactive power Q* changes from 0 to 0.1 pu. It is shown in the figure 15 that the PQ controller is used to make the converter's real and reactive power track the reference values. A higher value of k_i results in a faster response.
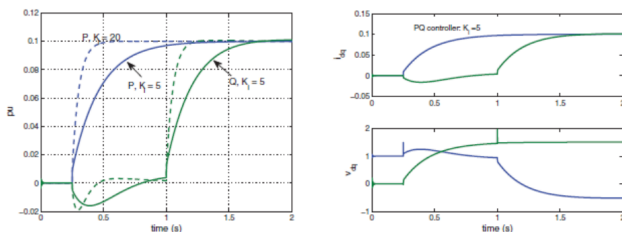

Fig. 15. Simulation results for PQ control blocks.

3.3. Designing of VF control loop
In an autonomous mode of operation, a converter can be operated in a VF control mode. The two main operations that a converter has to perform is to maintain PCC voltage to a reference value, to maintain the system frequency to a reference value. An example is shown in figure 16 that VSC is serving a load, the PCC voltage is the load voltage or the voltage across the capacitor.
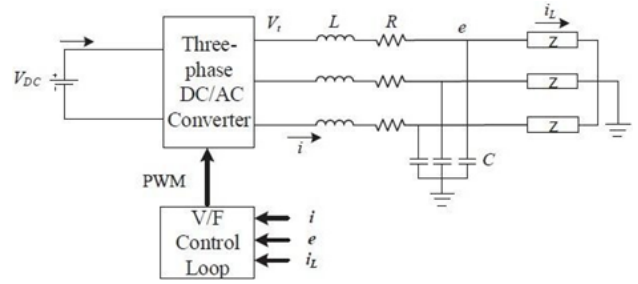

Fig. 16. An islanded microgrid with a VSC serving a load.

The main motive is to control the capacitor voltage. In both the modes of operation i.e., VF and PQ modes, inner current control loop is always present. In PQ control mode, the outer PQ control is used to track the current reference. VF control mode also used to track the reference currents. In order to derive the plant model, from figure 16 it is shown that the controller input is the capacitive voltage, and the output is the reference current , the plant is modelled to have current as input and the capacitive voltage as the output [12]. Taking an assumption that the inner current loop dynamics is faster than the outer loop. Thus, we can consider $i*_d \approx i*_d, i_q \approx i_q$

The dynamics of the capacitor is described both in abc frame as well as in dq frame:

$$C\frac{de}{dt} = i - i_L, abc \ frame \tag{22}$$

$$C\frac{d(e_d + je_q)}{dt} + j\omega C(e_d + je_q) = i_{Ld} - ji_q - (i_{Ld} + ji_{Lq}), in \ dq \ frame \tag{23}$$

Separating the real and imaginary parts of the equation in the dq frame, we get the equations in the d and q axis;

$$C\frac{de_q}{dt} - j\omega Ce_q = i_d - i_{Ld} \tag{24}$$

$$C\frac{de_q}{dt} + j\omega Ce_q = i_q - i_{Lq} \tag{25}$$

Taking the Laplace transform of the above equation, the linear control design is as follows:

$$\frac{e_d}{u_d} = \frac{e_q}{u_q} = \frac{1}{sC} \tag{26}$$

$$where, u_d = i_d - i_{Ld} + jwCe_q$$

$$u_q = i_q - i_{Lq} - jwCe_d \tag{27}$$

Taking simple first order plant model, PI controllers are designed to track the reference voltages $e*_d$ and $e*_q$. The outputs of the PI controllers are u_d and u_q. The reference currents can be calculated from the following relationships:

$$\begin{cases} i_d^* \approx i_d = u_d + i_{Ld} - jwCe_q \\ i_q^* \approx i_q = u_q + i_{Lq} + jwCe_d \end{cases} \tag{28}$$

The frequency of the three phase *abc* voltage can be set to the reference value. This can be achieved by giving the *dq/abc* conversion block an $\omega_o t$, angle where ω_o is the reference frequency.

The complete VF block diagram is shown in figure 17.

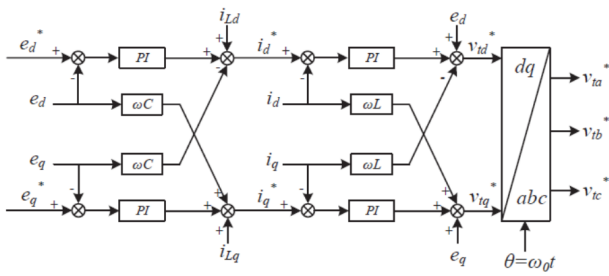**Fig.17.** VF control.

Fig. 19. Step response of VF controller.

3.4. Performance of VF control

A Simulink model of figure 17 is presented in figure 18. The model is built to validate the VF control performances. The block diagram consists of two parts: the circuit dynamics and control. The outputs of the circuit dynamics blocks are used for measurements of the converter currents i_d and i_q load currents. Outputs of the control blocks are the converter voltage v_d and v_q. In order to validate the circuit dynamics in *abc* frame *dq/abc* and *abc/dq* conversion blocks are required.

In this case, the circuit dynamics are modelled in *abc* frame. There are three state variables for each phase, the capacitor voltage, the converter currents and the load currents $_{iLj}$, where j =a,b,c. The differential equations related to the above state equations are as follows:

$$\begin{cases} C\frac{de_j}{dt} = i_j - i_{Lj} \\ L\frac{i_j}{dt} = v_{tj} - e_j - Ri_j \\ L_L\frac{di_{Lj}}{dt} = e_j - R_L i_{LK} \end{cases} \qquad (29)$$

The load is assumed to be a RL load with a resistance R_L and load inductance L_L.

In the Simulink block diagram, the state variables are taken from the outputs of the integrators. The block which is the inputs to the integrators are the derivatives of the state variables. It has inputs from two sources: Vabc from the converter block, iabc and ILbac from the output of the integrator.
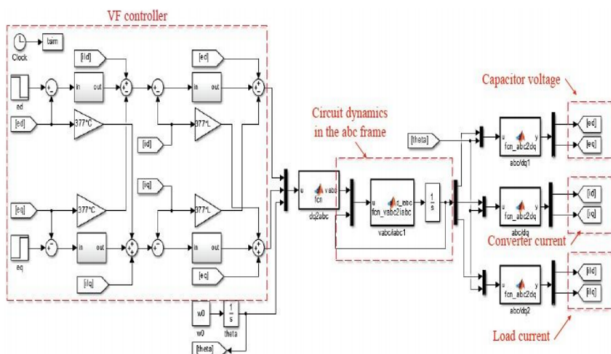

Fig. 18. A single VSC serving to a load using VF control.

Step response for the dq- axis voltages are also being studied. It is being studied that $e*_d$ is changed at t=0.05s while $e*_q$ is changed at t=0.1 s, the simulation results are shown in figure 19. It is seen that the two voltages track the reference in an efficient manner.
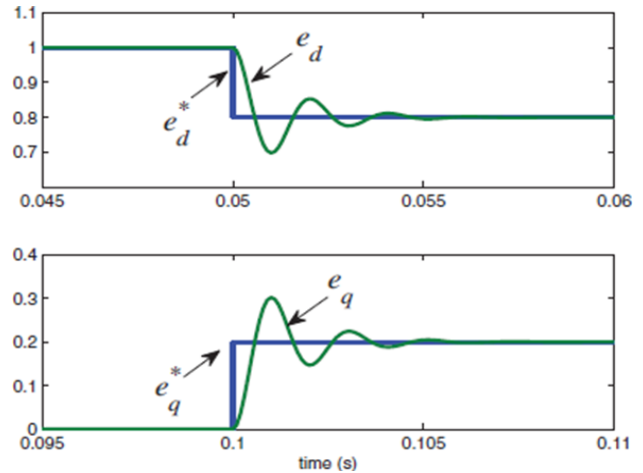
4. Result and Summary

4.1. P-F and Q-E droops

Various power sharing method among the converters are being discussed. Droop controls method which finds its application in synchronous generator. The droop control equations are as follows:

$$\begin{cases} \omega = \omega^* - m(P - P^*) \\ E = E^* - n(Q - Q^*) \end{cases} \qquad (30)$$

Where ω^* and E^* are the frequency and the magnitude of the output voltage of the converter.

The implementation of the droop control depends upon the converter mode. We have studied two type of control: PQ and VF. Droop control implementation is different for both type of control. Figure 20. shows the implementation of droop control in PQ and VF mode [13].
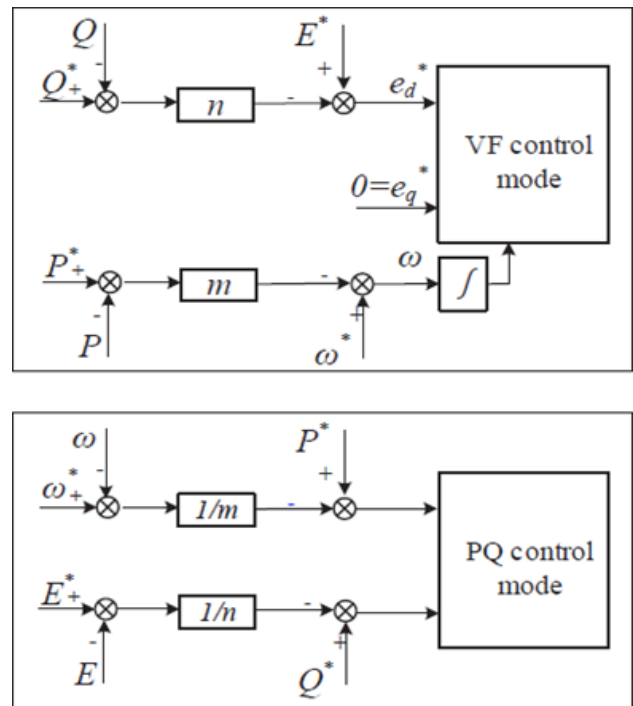

Fig. 20. Two different droop implementation.

4.2. Power sharing among two parallel converters in PQ control mode

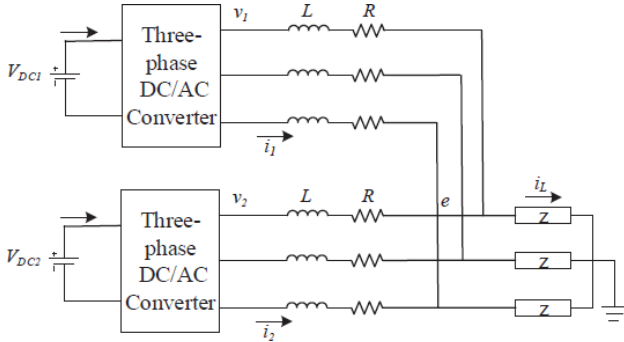Let's examine a model of two VSC feeding a load as shown

in figure 21.

Fig. 21. Two VSCs serving a load.

The VSCs are in PQ control mode. Besides PQ control mode, P-f and Q-E droops are applied. The voltage that is to be measured in Q-E mode is the PCC voltage. The frequency that is to be measured in P-f mode is the PCC frequency. A PLL is designed which will calculate PCC voltage and frequency. The Simulink diagram is shown in figure 22.

Initially, each VSCs share half of the real power i.e., 0.5 pu while the reactive power is zero as the load taken in this case is purely resistive. The droop coefficients are taken to be $m_1 : m_2 = n_1: n_2 = 1 : 2$, when there occurs a load change. When there is a change in load VSC_2 will take a load of while VSC_1 will share a load of 1/3 pu.

The PCC voltage is fixed at 1pu. Now we are decreasing the load resistance from 1.5pu to 1.2pu. With the reduction in the load resistance there is an increase in power supply by the converter from 1pu to 1.25pu. Since, there is a change of 0.25pu in real power, 0.167pu will get generated by VSC2 while 0.083 pu will get generated by VSC1. Therefore, the steady state value of VSC2 will be 0.667pu and VSC1 will be 0.583pu. The results are shown in figure 22. As load gets increased, there is reduction in system frequency.
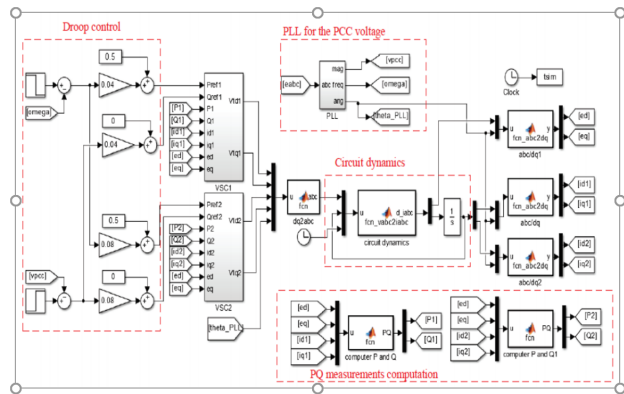

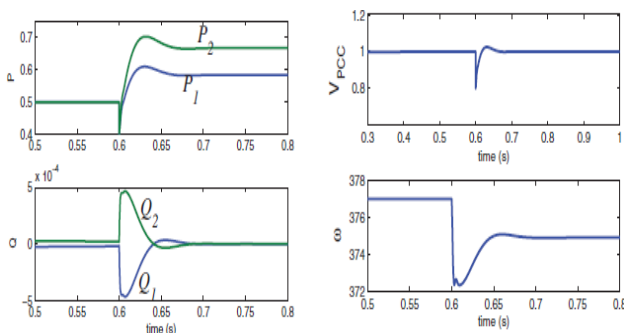**Fig. 22.** Two VSCs serving a load using droop control.

Fig. 23. Simulation results for load change at t=0.6s.

4.3. V-I droop
V-I droop design are mainly used for reactive power sharing. Converters which are interfaced with distributed energy resources, there is a need to design control for both real power and reactive power. V-I droop provides the facility for both real and reactive power sharing.
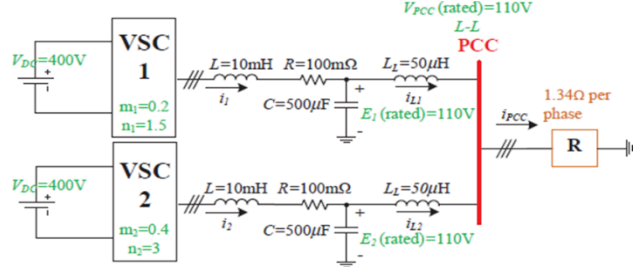

Fig. 24. Two DERs feed a load using parallel VSCs.

Taking two converters (which includes the RLC filter) are connected to the PCC bus connected through a RL impedance $R_j + X_j$, where j = 1,2 as shown in figure 24. The complex power injected to the load through the grid is noted as S_j, j=1,2. The complex power is expressed as:

$$S_j = \frac{3}{2}v_d(i_{Ldj} - ji_{Lqj}) = \frac{3}{2}v_d i_{Ldj} - v_d j i_{Lqj} \tag{31}$$

Therefore,

$$\begin{cases} P_j = \frac{3}{2}v_d i_{Ldj} \\ Q_j = \frac{3}{2}v_d i_{Lqj} \end{cases} \tag{32}$$

Thus, the d-axis currents calculate the real power distribution, and the q-axis current calculate the reactive power distribution [14]. At steady state, the PCC voltage, the converter voltage, and the currents are shown in the given relationship.

$$\begin{bmatrix} R_j & -X_j \\ X_j & R_j \end{bmatrix}\begin{bmatrix} i_{Ldj} \\ i_{Lqj} \end{bmatrix} = \begin{bmatrix} E_{jd} \\ E_{jq} \end{bmatrix} - \begin{bmatrix} v_d \\ 0 \end{bmatrix} \tag{33}$$

Applying the V-I control and assuming the droop coefficients as m_j for the d axis and n_j for the q axis, then the next relationship will become:

$$\begin{bmatrix} E_{jd} \\ E_{jq} \end{bmatrix} - \begin{bmatrix} v_d \\ 0 \end{bmatrix} = \begin{bmatrix} E_0 \\ 0 \end{bmatrix} - \begin{bmatrix} m_j & 0 \\ 0 & n_j \end{bmatrix}\begin{bmatrix} i_{Ldj} \\ i_{Lqj} \end{bmatrix} - \begin{bmatrix} v_d \\ 0 \end{bmatrix} \tag{34}$$

$$\Rightarrow \begin{bmatrix} R_j + m_j & -X_j \\ X_j & R_j + n_j \end{bmatrix}\begin{bmatrix} i_{Ldj} \\ i_{Lqj} \end{bmatrix} = \begin{bmatrix} E_0 \\ 0 \end{bmatrix} - \begin{bmatrix} v_d \\ 0 \end{bmatrix}$$

Assuming, $m_j >> R_j$, $n_k >> R_j$, $m_j >> X_j$, $n_j >> X_j$ then the following relationship becomes:

$$\begin{cases} m_1 i_{Ld1} = m_2 i_{Ld2} \\ n_1 i_{Ld1} = n_2 i_{Ld2} \end{cases} \tag{35}$$

Thus, the real power distribution is proportional to $1/m_j$ and the reactive power distribution is proportional to $1/n_j$ when we take a resistive type of network i.e., $R_j >> X_j$ then the real power distribution is proportional to $1/ (R_j + m_j)$ and the reactive power distribution is proportional to $1/ (R_j + n_j)$. If we take the droop coefficients m_j and n_j comparable with R_j and X_j, then accurate real/reactive power sharing will be

difficult to determine. But if we take very large droop coefficients, it will make the converter voltage drop to a low value during heavy load conditions.

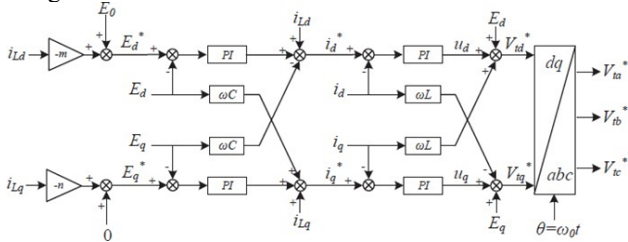The control block diagram for the V-I control is shown in figure 25.

Fig. 25. Block diagram for V-I droop.

The basic control is in charge of maintaining the right load distribution among the distribution generation units, balancing production and consumption, and regulating and stabilizing the frequency and voltage in the microgrid. The key control approaches were thoroughly addressed in this research. It is clear that every control strategy has benefits and drawbacks of its own. The comparison of droop and communication control is given in the Table 1.

Table 1. Comparison of droop and communication control methods

Droop control	Communication control
• Droop based techniques use local measurements of the system characteristics to give the distributed generation units a genuinely distributed functioning. • For dependable operation, they don't rely on cables. • Numerous beneficial chaacteristics of droop-based approaches include the system being modular, flexible, redundant, expandible. • Owing to the impedance of line, there are few limitations, such as variation in frequency and voltage amplitudes, inverter circulating currents and most importantly delayed transient responses.	• The communication based approaches offer precise power distribution, quick transient reaction, good power quality, and reduced power circulation of currents in inverter. • These techniques require communication links having higher bandwidth for their implementation. • It is difficult to upgrade the network because we should be knowing the number of inverters present in the microgrid and we also be knowing the values of load currents. • The necessary inter-connection makes the network less reliable and prevent it from being genuinely distributed and redundant.

5. Conclusion

The control structure of VSC has been presented implemented in MATLAB software. VSC structure in cascaded form is used. Different schemes for real and reactive power sharing are being implemented. An inner current controller is designed. After inner current loop is implemented phased locked loop (PLL) is designed which is used to identify the change in frequency of the input signal and correct it. It is also used to track the input angle. The outer loop is made which has a slower response than the inner loop.

PQ controller is designed which makes the converter real and reactive power to track the reference values. Another scheme VF control is studied in which it is concluded that the control designed is efficiently track the dq voltages to the reference values. Power sharing between the converters is studied using PQ mode. It is verified from the Simulink model that as the load gets increased, there is a reduction in system frequency.

_____

References

1. I. Akhtar, W. U. H. Paul, S. Kirmani, and M. Asim, "Cost Analysis of 18 kW Solar Photovoltaic System for Smart Cities Growth in India," in *Lecture Notes in Electrical Engineering*, 723 (1), pp 661-668.
2. M. U. Bashir, W. U. H. Paul, M. Ahmad, D. Ali, and Md. S. Ali, "An Efficient Hybrid TLBO-PSO Approach for Congestion Management Employing Real Power Generation Rescheduling," *Smart Grid and Renewable Energy*, 12(8), 2021, pp. 113–135.
3. M. Ahmad, D. Ali, W. U. H. Paul, M. S. Ali, and H. Ashfaq, "Management of Energy and Coordinated Control of PV/HESS in Islanded DC Microgrid", *Smart Energy and Advancement in Power Technologies*, 1(1), 2023, pp. 325–339.
4. D. Ali, W. U. H. Paul, M. S. Ali, M. Ahmad, and H. Ashfaq, "Optimal Placement of Distribution Generation Sources in Hybrid Generation Network," *Smart Grid and Renewable Energy*, 12(5), 2021, pp. 65–80.
5. Md. S. Ali, A. Ahmad, W. U. H. Paul, D. Ali, and M. Ahmad, "Optimal Allocation of Wind-Based Distributed Generators in Power Distribution Systems Using Probabilistic Approach,",*Smart Energy and Advancement in Power Technologies*, 1(1), 2023, pp. 385–396.
6. N. W. A. Lidula and A. D. Rajapakse, "Microgrids research: A review of experimental microgrids and test systems," *Renewable and Sustainable Energy Reviews*, 15(1), 2011, pp. 186–202.
7. T. S. Ustun, C. Ozansoy, and A. Zayegh, "Recent developments in microgrids and example cases around the world—A review," *Renewable and Sustainable Energy Reviews*, 15(8), 2011, pp. 4030–4041.
8. P. M. Costa and M. A. Matos, "Assessing the contribution of microgrids to the reliability of distribution networks," *Electric Power Systems Research*, 79(2), 2009. pp. 382–389.
9. J. J. Justo, F. Mwasilu, J. Lee, and J.-W. Jung, "AC-microgrids versus DC-microgrids with distributed energy resources: A review," *Renewable and Sustainable Energy Reviews*, 24(1), 2013 pp. 387–405.
10. W. U. H. Paul, S. Kirmani, M. B. Bhat, and S. A. Nahvi, "Data Based Controller Design for PMDC Motor Setup using System Identification," *Studies in Indian Place Names*, 40(10), 2020, pp. 11-18.
11. A. T. Elsayed, A. A. Mohamed, and O. A. Mohammed, "DC microgrids and distribution systems: An overview", *Electric Power Systems Research,* 119(1) 2015, pp. 407–417.

12. Y. Chen, J. Zhao, J. Wang, K. Qu, S. Ushiki, and M. Ohshima, "A decupled PQ control strategy of voltage-controlled inverters, "In: *9th International Conference on Power Electronics and ECCE Asia* (ICPE-ECCE Asia),.2015, pp. 1374–1379.

13. M. Naresh and R. K. Tripathi, "Power flow control and power quality issues in distributed generation system," In 2016 IEEE 1st *International Conference on Power Electronics, Intelligent Control and Energy Systems (ICPEICES),* 2016, pp. 1–5.

14. Yalong Wei, Hui Zhang, Qiong Song, and Kai Sun, "Control strategy for parallel-operated virtual synchronous generators," in *IEEE 8th International Power Electronics and Motion Control Conference (IPEMC-ECCE Asia),* 2016, pp. 2015–2021.

15. K. Shi, W. Song, P. Xu, R. Liu, Z. Fang, and Y. Ji, "Low-Voltage Ride-Through Control Strategy for a Virtual Synchronous Generator Based on Smooth Switching," *IEEE Access,* 6(1), 2018, pp. 2703–2711.

16. Z. Liu and J. Liu, "A novel control strategy of inverter in distributed

generation with seamless transfer capability," In: *Twenty-Sixth Annual IEEE Applied Power Electronics Conference and Exposition (APEC),* 2011, pp. 1594–1598.

17. B. Dong, Y. Li, and Z. Zheng, "Control strategies of DC-bus voltage in islanded operation of microgrid," In: *4th International Conference on Electric Utility Deregulation and Restructuring and Power Technologies (DRPT),* 2011, pp. 1671–1674.

18. S. Lissandron and P. Mattavelli, "A controller for the smooth transition from grid-connected to autonomous operation mode," In *IEEE Energy Conversion Congress and Exposition (ECCE),.* 2014, pp. 4298–4305.

19. X. Ma, P. Yang, H. Dong, J. Yang, and Y. Zhao, "Secondary control strategy of islanded micro-grid based on multi-agent consistency," In: *IEEE Conference on Energy Internet and Energy System Integration (EI2),* 2017, pp. 1–6.